Improved quantitative calibration of rock physics models

Bernardo Moyano[1], Erling Hugo Jensen[1], Tor Arne Johansen[1,2].

ABSTRACT

In reservoir characterization, rock-physics models provide the link between seismic observables (density, compressional and shear wavespeeds) and reservoir parameters such as porosity, lithology and fluid saturation. However, the accuracy of these predictions is rarely explored. In fact, the validation of a model representing a dataset is often limited to the analysis of a cross-plot of two arbitrary magnitudes. The objective of this paper is to improve the calibration procedure through a quantitative assessment of the reservoir property predictions using various rock-physics models. The analysis is based on an inverse rock-physics modelling that organizes the rock-physics transforms into constraint data so that the seismic variables are direct functions of the reservoir parameters. It is revealed that the predictions of reservoir quality can assist in the diagnosis of the rock microstructure itself, such as the location of clay particles in clay-rich sediments. In addition, we found that a quantitative analysis is the only way to evaluate accurately the performance of various models when studying heterogeneous datasets.

INTRODUCTION

Selecting and calibrating the most suitable rock-physics model for a given dataset is an exercise with a non-unique solution. Rock-physics models capture one or a select few factors that influence the elastic properties of the rocks. In addition, these models typically are calibrated to a limited set of physical data (e.g. compressional (P) velocity data). One group of models based on contact theory (Mindlin 1949) treats rocks as a collection of grains and estimates their stiffnesses from the contact stress between two spheres of equal size. On the other hand, inclusion models (Berryman 1980) treat the rock as an elastic solid with cavities and accounts for the effects of shapes of multiple pores on elasticity. In practice, general guidelines and additional observations help to constrain the model space to a relatively small number of plausible options. For example, contact models have been used successfully to study the pressure dependence of velocity of unconsolidated sediments (Dvorkin & Nur 1996). Inclusion models are often preferable when analyzing well-

[1] Department of Earth Science, University of Bergen, Bergen, Norway.
[2] NORSAR, Bergen, Norway.

consolidated rocks (Sheng 1990; Berge *et al.* 1993). However, after selecting a modelling strategy, we are frequently left with several possible models that seem to represent experimental data equally well.

In reservoir characterization, the ultimate goal of a rock-physics model is to assist in the inversion of seismic data for porosity, lithology and pore fluid (PLF). These models define the transforms between seismic observables and reservoir parameters. Selecting a specific model implicitly defines the dominant parameters that control these relationships and determines the accuracy of the predictions. Therefore, a crucial step is to calibrate and to compare the predictions quantitatively when more than one model appears equivalently valid for a given area.

Various models are used to account for the dependence of elastic properties on different physical conditions. Pressure dependence has been captured by models based on contact theory (Mindlin 1949; Digby 1981; Walton 1987). The stiffness effect due to cement located at the grain contacts is often calculated using contact cement theory (Dvorkin & Nur 1996), whereas pore microstructure effects can be modelled by inclusion models (Kuster & Toksoz 1974; Berryman 1980). Self-consistent approximations (O'Connell & Budiansky 1974; Hornby *et al.* 1994; Berryman 1995) and differential effective medium (DEM) models (Berryman 1992) have been developed specifically to extend inclusion models to handle higher concentrations of inclusions. Shales, due to their complex lithology and reduced pore sizes have been idealized through inclusion models, (Hornby *et al.* 1994; Jakobsen *et al.* 2003; Johansen *et al.* 2004a; Draege *et al.* 2006). The equations of Gassmann (1951) simulate the low-frequency effects of different pore fluids on seismic velocities. Avseth *et al.* (2010) provide an overview of theoretical, empirical, heuristic and hybrid strategies to model diagenetic and depositional trends in unconsolidated high-porosity sediments. Thus, ambiguities can arise when we apply various models to estimate simultaneously reservoir properties such as lithology, porosity and saturation. Little work has been done to evaluate systematically PLF parameters obtained using different models. For a given dataset, the selection of a rock-physics model is uncertain, in terms of providing the most suitable relationship between the seismic and PLF parameters. The goal of this paper is to present a way to select and calibrate the most suitable rock-physics model for a given dataset and reduce the non-uniqueness of the reservoir characterization problem. We do this by quantifying the accuracy of different rock-physics models in the prediction of reservoir parameters when calibrated to experimental data. We use an approach (Johansen *et al.* 2004b) that organizes the rock-physics transforms into constraint data where the seismic variables (e.g., velocity and density) are direct functions of the selected PLF parameters. We start with a review of this strategy, and then we demonstrate the calibration procedure in two cases using real data. In case 1 we use the procedure to illustrate the shortcoming of the traditional cross-plot type of calibration. We do this by comparing the reservoir property predictions made with a model for dispersed clay (Dvorkin & Gutierrez 2001)

versus a model for structural clay (Avseth *et al.* 2005) on a set of laboratory measurements of clay-sand composites (Yin 1992). In case 2 we explore the accuracy of various rock-physics predictions of reservoir properties considering a more extensive dataset (Han *et al.* 1986). Subsequently, we select the most suitable models and then perturb individual parameters to optimize the final predictions.

INVERSE ROCK PHYSICS MODELLING

A common practice in rock-physics analysis is to use cross plots to study trends and property dependencies. For example, Figure 1a shows the predicted bulk modulus versus porosity trends for a particular fluid saturation and different lithologies using a rock physics model. In the strategy of Johansen *et al.* (2004b) such modelled dependencies are resampled into a scalar field of the reservoir properties. Figure 1b illustrates the resampling of two bulk moduli values into a lithology versus porosity cross plot. Repeating this for the other moduli values and various fluid saturations gives us the 3D cube in Figure 2. The resampled bulk modulus can be thought as a scalar field *K.* In this case, $K = K(\phi, C, S)$, where ϕ, C and S denote the porosity, clay and fluid volume fractions, respectively for a particular rock physics model. From $K(\phi, C, S)$, we calculate a numerical relationship between ϕ, C and S which corresponds to a specific bulk modulus value. For the 3D cube this typically produces a surface that we denote an iso-surface because all points on this surface correspond to the same modulus.

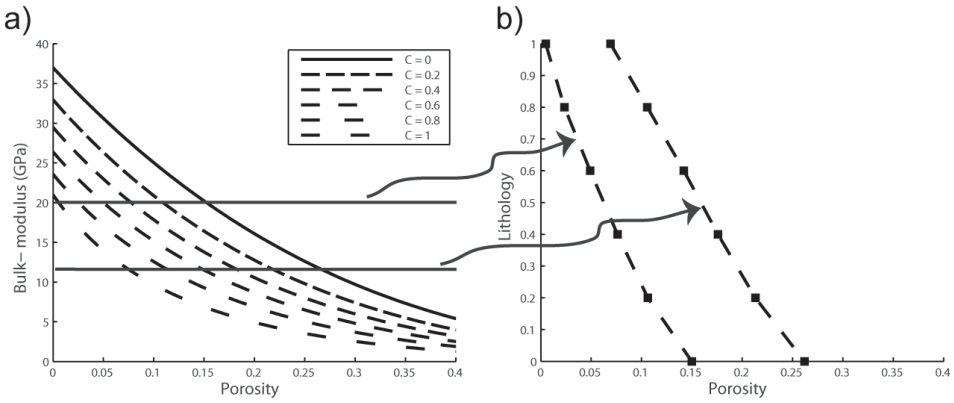

Figure 1 Resampling of a rock-physics model from velocity-porosity to lithology-porosity space. C_i are model results for various clay contents.

Estimating reservoir properties

An iso-surface can be used to study predicted reservoir property dependencies for a particular seismic parameter value and a given rock physics model. Any combination of ϕ, C and S corresponding to a point on such a surface is a possible solution for the particular seismic parameter value. Typically, we have data of more than one seismic parameter (compressional and shear wavespeeds, V_p and V_s, and bulk density ρ), and by combining their individual iso-surfaces we constrain the possible PLF solutions. A combination of two seismic observables (e.g. V_p and ρ) will normally lead to one or more curving lines in the PLF domain. Furthermore, a combination of three observables leads to one or more point solutions because we are dealing with a non-linear problem (see Figure 3). Another possible outcome of the inversion is that no intersection is found, i.e., no combination of reservoir properties is consistent with the set of observables. This means that the selected rock physics model fails to reproduce the data and other possible model candidates should be tested.

When working with real data, it is difficult to find a rock physics model that is able to predict the correct reservoir properties for every data point unless uncertainty is included. In case one, we include a few perturbed values of the input data in addition to the observed data and perform the inverse modelling. In the second case, we handle the uncertainty by using a so-called proximity based implementation of the inversion strategy. Here, the iso-surfaces are made up of densely sampled points. Intersections are identified when the points on one surface are within a maximum distance δ from points on another surface.

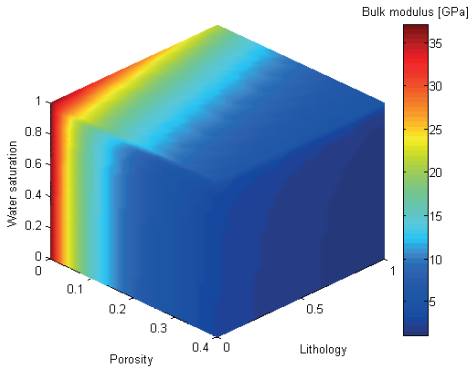

Figure 2 Bulk modulus constraint cube in the porosity, lithology, fluid space (PLF). The vertical axis is water saturation. The lithology axis varies from pure quartz (zero) to pure clay (one).

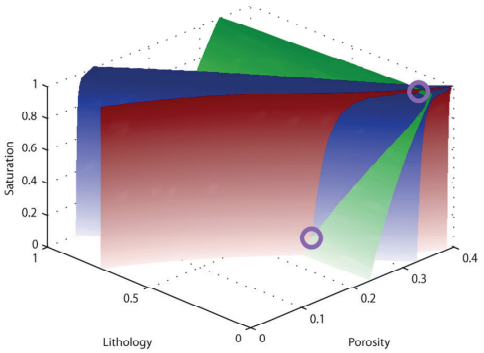

Figure 3 Three observations (Vp, Vs and density iso-surfaces) intersecting in the PLF space. Solutions exist at the two indicated points.

This maximum distance represents an absolute tolerance interval for the modelled ϕ, C and S. A sensitivity analysis of the applied models to the uncertainties in the measured rock properties can be made to derive a suitable tolerance interval for a given dataset. These point solutions are expanded to spherical point clouds with a radius $\delta/2$. An example of the inversion in Figure 3 using the proximity based implementation and a $\delta = 0.02$, is shown in Figure 4.

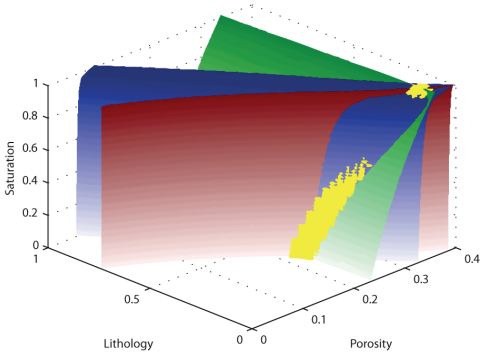

Figure 4 Three observations (Vp, Vs and density) intersecting in the PLF space. Uncertainty is implicitly handled by the proximity based implementation of the inverse modelling, providing a cloud of solutions as opposed to points as in Figure 3.

The calibration procedure

In the quantitative calibration of rock-physics models we compare predicted reservoir properties, i.e. axis readings at the intersecting points, to measurements of these properties from laboratory or well-log data. Through this analysis in the PLF space, we evaluate how accurate a model predicts reservoir properties from seismic data. In addition, we compare the predictions of reservoir properties from different models and discard those models that provide less accurate predictions. During the calibration process we can also maximize the tolerance in the intersections and quickly test the performance of several models, discard the less effective ones, and continue with the most promising ones. As the number of models is reduced to three or four, the uncertainty in the observations can be constrained to perform a more rigorous analysis. Finally, when the most suitable model has been identified, the same methodology can be repeated for various values of model parameters (aspect ratio, pressure, etc.) to optimize the calibration and improve prediction results. We applied this methodology to quantify the calibration of various rock-physics models to two datasets of clay-rich sandstones.

CASE 1: EVALUATING CLAY DISTRIBUTION IN CLAY-SAND COMPOSITES

We applied the methodology to a laboratory dataset of clay-sand composites prepared by Yin (1992). The samples consist of mixtures of pure kaolinite and Ottawa sand with a grain size ratio of 1/20, providing an ideal binary mixture. For low quantities of clay, the small clay particles likely occupy part of the pore space of the larger sand particles (a pore-

filling clay). This spatial distribution has a minimal effect on the structure of the composite. The dataset for 50 MPa of effective pressure is shown in Figure 5 where a reduction in porosity and increase in velocity are observed for increasing clay content. An overturned V-shape trend produced by the transition between sand and shale has been noted in the literature as an indicator of dispersed clay topology (Marion *et al.* 1992). In the context of rock-physics modelling, we denote shale as a fine-grained rock (clay-sized and silt-sized) in which clay minerals are the load-bearing phase. We calibrated a model for dispersed clay, and a model that is suitable for both structural and laminated clay to the dataset.

The model for dispersed clay (Dvorkin & Gutierrez 2001) is a velocity-porosity relationship that uses the Hashin-Shtrikman (HS) lower bound (Hashin & Shtrikman 1963) as a mixing law between two end members. The high-porosity end member is clean sand whose velocity is computed by contact theory (Mindlin 1949). The low-porosity end member represents the same sand with its pore space completely filled by clay. The porosity at this point is not zero because clay particles have intrinsic porosity. This is sometimes referred to as sand at critical clay content (Yin 1992). Dvorkin & Gutierrez (2001) computed this intermediate member by adding silt particles (quartz) to a pure shale also using the HS lower bound. The model consists of two domains. In the first domain, clay is the load-bearing phase (sandy-shale), whereas in the second domain, the sand pack is load bearing (shaley-sand), as in Figure 6.

In our modelling we focused on the shaley-sand section in which clay particles fill the pore space of the clean sand without significantly affecting its stiffness. Therefore, the

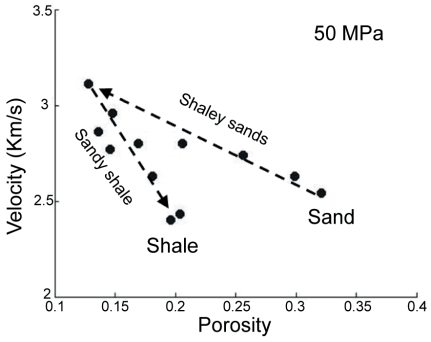

Figure 5 P-wave velocity versus porosity trend of clay-sand composites at constant pressure prepared by Yin (1992). Dashed arrows indicate increasing clay content. The V-shaped trend of increasing clay content, producing an increase of velocity (and a decrease in porosity) until clay content equals sand porosity, has been attributed to a pore filling clay topology.

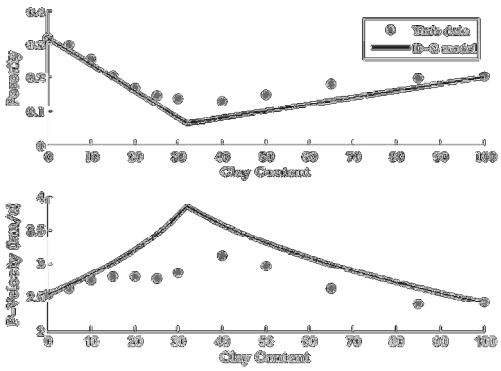

Figure 6 Dispersed clay model (Dvorkin-Gutierrez) calibrated to Yin's data. Note porosity is modelled well, but velocity is in general over-estimated. The model predicts that clay mineral becomes load-bearing (porosity minimum and velocity maximum) at about 30 % clay content.

properties of the mixture can be computed from the lower HS bounds of the clean sand and the sand at critical clay content. The elastic moduli of a shaley-sand with increasing clay content (C) are expressed as:

$$K_{MIX} = \left[\frac{1 - C/\phi_{ss}}{K_{ss} + (4/3)\mu_{ss}} + \frac{C/\phi_{ss}}{K_{cc} + (4/3)\mu_{ss}} \right]^{-1} - \frac{4}{3}\mu_{ss}\,, \tag{1}$$

$$\mu_{MIX} = \left[\frac{1 - C/\phi_{ss}}{\mu_{ss} + Z_{ss}} + \frac{C/\phi_{ss}}{\mu_{cc} + Z_{ss}} \right]^{-1} - Z_{ss}\,, \tag{2}$$

$$Z_{ss} = \frac{\mu_{ss}}{6}\left(\frac{9K_{ss} + 8\mu_{ss}}{K_{ss} + 2\mu_{ss}} \right), \tag{3}$$

where, K_{cc} and μ_{cc} are computed from the sandy-shale model at critical clay content. K_{ss}, μ_{ss} and ϕ_{ss} are the effective moduli and porosity of the clean sandstone.

In contrast, the constant clay model assumes the clay particles are located in the frame of the rock, reducing its overall stiffness. The model uses contact theory and the HS lower bound to model sands with a constant clay-quartz ratio in the velocity-porosity space (Avseth *et al.* 2005). This is suitable for sands with both structural and laminated clay. As Yin's dataset is composed of synthetic clay-sand aggregates we do not expect any laminations to be present and we refer to this as the model for structural clay. It is analogous to the unconsolidated sand model (Dvorkin & Nur 1996) but with a reduced critical porosity because a clay rich sand has lower critical porosity than a clean sand. The mineral point is computed by Hill's (1952) average of quartz and clay mineral moduli.

Conventional calibration

A conventional calibration consists of a qualitative fit of modelled curves for a given cross-plot domain. We calibrated both models to the dataset in the velocity-porosity space (Figure 7). The dispersed clay model matches well the clean sand and pure clay end members, but it misses the intermediate values of clay content. The structural clay model reproduces the variability of the P-wave velocity data, but its accuracy is difficult to evaluate. Note that the shear velocity data show no sensitivity to clay content.

In Figure 6, the dispersed clay model reproduces the decrease of porosity for increasing clay content shown by the data, and predicts a change in the load-bearing phase, from grain to matrix supported, for a clay volume of approximately 32%. Both models can be used to explain the data and to infer the internal organization of the clay particles in the

samples. However, we cannot determine which model explains the data better, nor, from these results, can we quantify how successfully either model represents the data.

Quantitative analysis in the PLF space

For the quantitative analysis, we used seven samples each with clay content <30%. When considering the intersections between three iso-surfaces for density, P- and S-wave velocities, we obtained a solution for only the pure sand sample, which constitutes a calibration point. This is due to the anomalous behaviour of shear velocities that none of the models could satisfactorily describe (Figure 7). Therefore, we continued using only P-wave velocity and density, ignoring S-wave velocity measurements. A comparison of the results can be seen in Figure 8, where the structural clay model produced solutions for the seven samples, good estimates of the porosity and less accurate estimates for lithology. On the contrary, the dispersed model found solutions for only four samples; three accurate in porosity and two in lithology.

If we include +/- 5 percent uncertainty in the P-wave velocity, the inverse modelling provides more solutions (see Figure 9). In this case the dispersed-clay model improves its performance and produces solutions for all seven samples with varying accuracy. The structural clay model also provides an increased number of solutions and shows a robust set of porosity and lithology predictions. A quantitative comparison of the modelling is

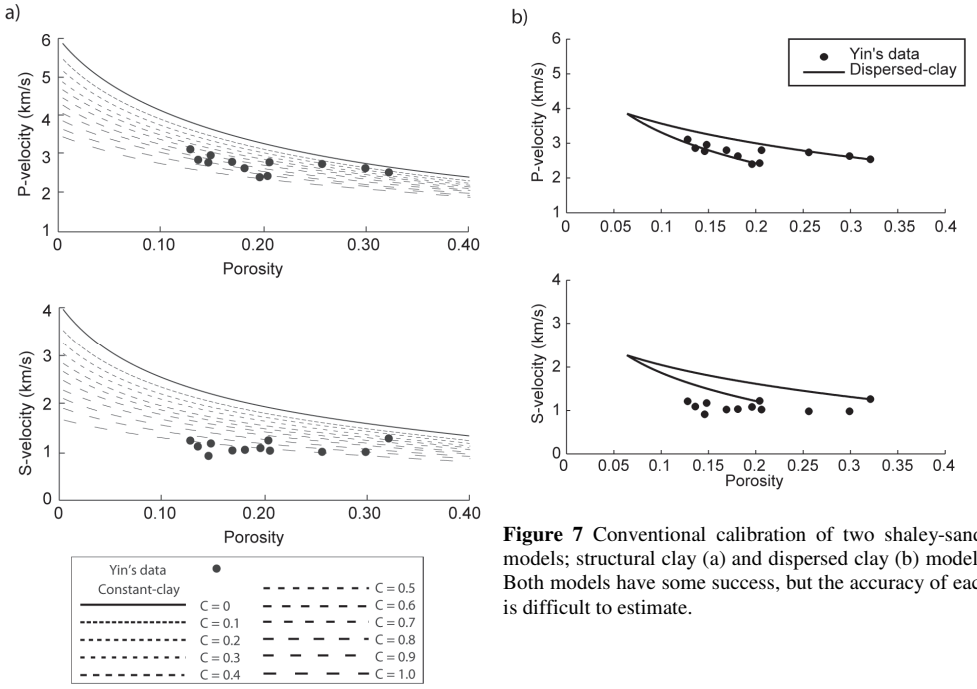

Figure 7 Conventional calibration of two shaley-sands models; structural clay (a) and dispersed clay (b) models. Both models have some success, but the accuracy of each is difficult to estimate.

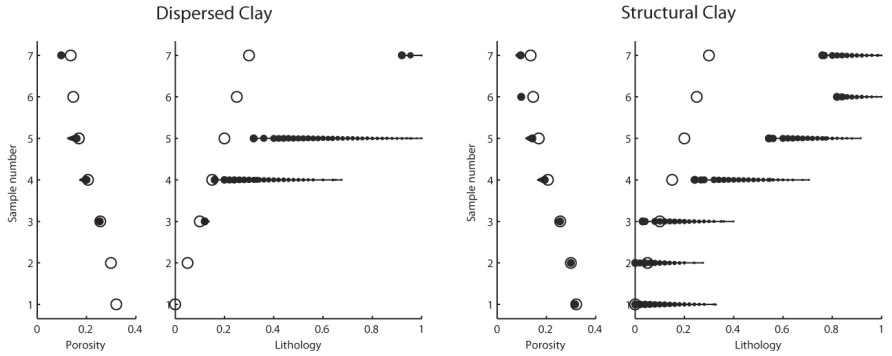

Figure 8 Quantitative calibration of dispersed clay (left) and structural clay (right) models. Vertical axis is sample number, empty circles are lab measurements and filled circles model predictions. Only 7 samples with clay content below 0.3 were used. Of the two models, the structural clay model produced more solutions.

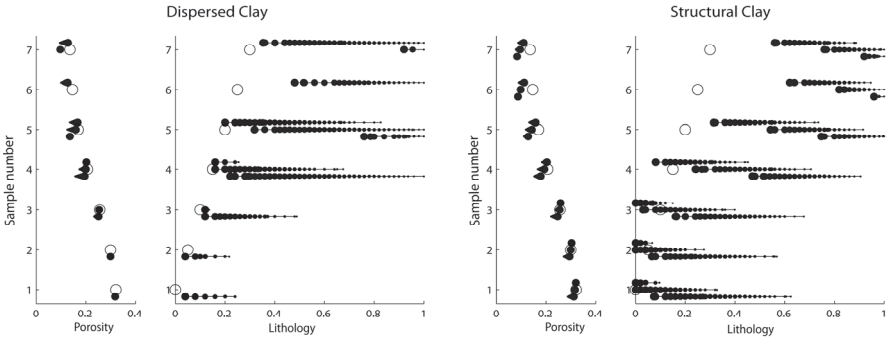

Figure 9 Quantitative calibration of the dispersed clay model (left) and structural clay model (right), using 5% uncertainty in *V*p. Vertical axis is sample number, empty circles are lab measurements and filled circles model predictions. More solutions were found relative to the results (Fig. 8) in which uncertainty was not included.

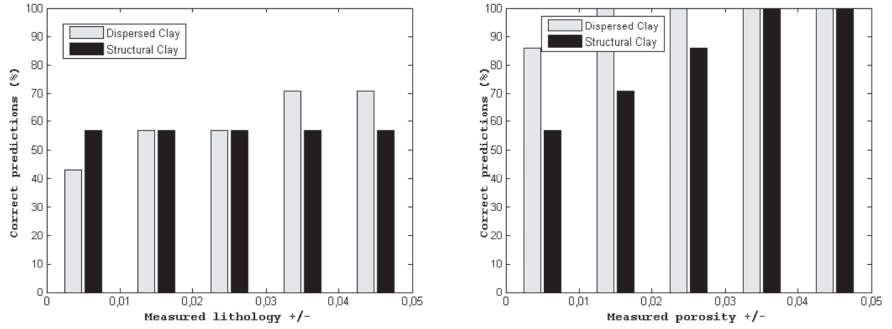

Figure 10 Quantitative calibration of dispersed clay (grey) and structural clay (black) models, using a 5 % of uncertainty in Vp. Vertical axis is percentage of predictions matching the data, versus various tolerance ranges in porosity and lithology predictions (+/– 0.01, 0.02, 0.03, 0.04, 0.05) in the horizontal axis.

shown in Figure 10, with the percentage of correct predictions along the vertical axis, and various tolerance ranges between observed and modelled porosities and lithologies (+/− 0.01, 0.02, 0.03, 0.04, 0.05) along the horizontal axis. Figure 10 shows that the two models predict similarly well the lithology, whereas the porosity is more precisely estimated by the dispersed clay model. However, Figures 8 and 9 show that the dispersed clay model is more sensitive to the uncertainty of the P-wave velocity.

CASE 2: VALIDATING ROCK-PHYSICS MODELS FOR CLAY-RICH SANDSTONES

In this case we assessed the calibration of various models to a larger dataset based on 80 sandstone samples with wide ranges of porosity, age and clay content (Han et al. 1986). We started by exploring three models. One is a granular model based on contact theory combined with HS bounds and the other two are inclusion models.

The first model is referred to as the modified Hashin-Shtrikman upper bound (MHS) and uses Hertz-Mindlin (Mindlin 1949) theory to compute a clean, high-porosity sand and an HS upper bound to estimate lower porosities towards the mineral point. This model has been used to describe a mixture of sediment deposited at critical porosity with some additional mineral. It mimics the steep diagenetic trend of clean sands in the velocity-porosity space (Avseth *et al.* 2005). For clay-rich data, it connects a lower critical porosity member with softer effective mineral moduli. We used quartz mineral properties, K_q = 37 GPa, μ_q = 44 GPa for bulk and shear moduli, and clay properties computed for this dataset K_c = 25 GPa and μ_c = 9 GPa (Han *et al.* 1986). Effective pressure was 40 MPa, nine contact points per grain on average (coordination number), and we assumed critical porosity to decrease linearly between 0.4 for clean sand and 0.2 when clay content is 1.

Then, we applied the model of Xu & White (1995) for clay-sand mixtures, which divides the pore space into sand related pores (stiff) and clay related pores (compliant), assigning different aspect ratios to them. For implementation we used a non-interaction approximation (Hudson & Knopoff 1989; Hornby *et al.* 1994) to compute the effective compliance tensor $\mathbf{S}^*$ from those of the host rock $\mathbf{S}^0$ and the pore space as:

$$\mathbf{S}^* = \mathbf{S}^0 - \sum_{n=1}^{N} v_n \left(\mathbf{S}^0 \mathbf{C}^n - \mathbf{I}\right) \mathbf{K}^n , \tag{4}$$

$$\mathbf{K}^n = \left[\mathbf{C}^0 \left(\mathbf{I} + \mathbf{G}^n \left(\mathbf{C}^n - \mathbf{C}^0\right)\right)\right]^{-1}. \tag{5}$$

In equations 4 and 5, $\mathbf{S}^*$ is the effective compliance tensor; $\mathbf{S}^0$ the compliance tensor of the isotropic host rock; v_n is the volume concentration of the nth phase; and $\mathbf{I}$ is the identity

tensor. The factor $\mathbf{G}^n$ is a fourth-rank tensor that depends on the stiffness tensor of the host rock ($\mathbf{C}^0$) and the shape/orientation of the n^{th} inclusion type that characterizes the elastic effect of individual inclusions. The excess compliance due to the pore space includes contributions of sand related pores (α_{stiff}) and clay related pores (α_{soft}). Aspect ratios of α_{stiff} = 0.1 for sand and α_{soft} = 0.05 for clay related pores were initially applied. The effective stiffness tensor is then obtained by inverting the effective compliance tensor. The effect of the fluid is computed using Gassmann's (1951) equations. Increasing clay content means increasing number of compliant pores and results in a softening of the effective properties of the rock.

The third model used differential effective medium (DEM) theory (Berryman 1992) to introduce empty isolated pores with a constant aspect ratio (α = 0.25) into a mineral host medium. This requires solving a coupled system of ordinary differential equations:

$$(1-y)\frac{d}{dy}\left[K^*(y)\right]=\left(K_2-K^*\right)P^{(*2)}(y)\ , \tag{6}$$

$$(1-y)\frac{d}{dy}\left[\mu^*(y)\right]=\left(\mu_2-\mu^*\right)Q^{(*2)}(y)\ , \tag{7}$$

where K^* and μ^* are the effective bulk and shear moduli, $K^*(0) = K_1$ and $\mu^*(0) = \mu_1$ are the effective elastic moduli at initial conditions (initial host material), K_2, μ_2 and y denote the moduli and concentration of the added inclusions. The terms P^* and Q^* are geometrical factors associated with the inclusion material. The fluid effect was again introduced using Gassmann's equations (Gassmann 1951).

All three models provided a satisfactory calibration in the velocity-porosity space for P- and S-velocities (Figure 11), but a quantitative analysis is required to evaluate and compare their successes further.

QUANTITATIVE ANALYSIS IN PLF SPACE

The quantitative analysis in the PLF space for the three models is summarized in Figure 12. All three models show similar porosity predictions, but lithology estimations by the DEM consistently under-performs. Hence, we discarded the DEM model and focused the quantitative analysis on the other two models (MHS and XW). A comparison between their results from the intersections of Vp, Vs and density iso-surfaces is shown in Figure 13. The empty circles represent (laboratory) measurements, and the filled circles are our modelling results. There is more than one prediction for each sample (vertical axis). Furthermore, for every porosity prediction, a corresponding lithology prediction exists, indicated in the figure by the size of the filled circles. The radius of the filled circles increases with

decreasing clay content. An inspection of Figures 12 and 13 shows that both model predictions are similar in number and accuracy, with a slight advantage for the MHS model. Therefore, we performed a sensitivity analysis on one key parameter for each of the models. We tested coordination numbers between 8 and 10 for the MHS model and various combinations of aspect ratios in the XW model. The MHS model shows stable results in terms of coordination number (C), but slightly favouring C = 8 over the other (Figure 14). To analyze the XW model we used five different models (1 to 5) with aspect ratios of sand and clay pores (α_{sand} , α_{clay}) as follows: M1 = (0.1, 0.035); M2 = (0.1, 0.06); M3 = (0.12, 0.035); M4 = (0.12, 0.05); M5 = (0.12, 0.06): see Figure 15. Porosity predictions of the XW model were highly dependent on the aspect ratios of sand and clay pores, whereas lithology estimations were less sensitive. This analysis demonstrated that the lithology results were improved when using aspect ratios of α_{sand} = 0.12 and α_{clay} = 0.035 (model 3). However, better porosity estimations were achieved with slightly stiffer clay pores (models 4 (α_{clay} = 0.05) and 5 (α_{clay} = 0.06) in Figure 15).

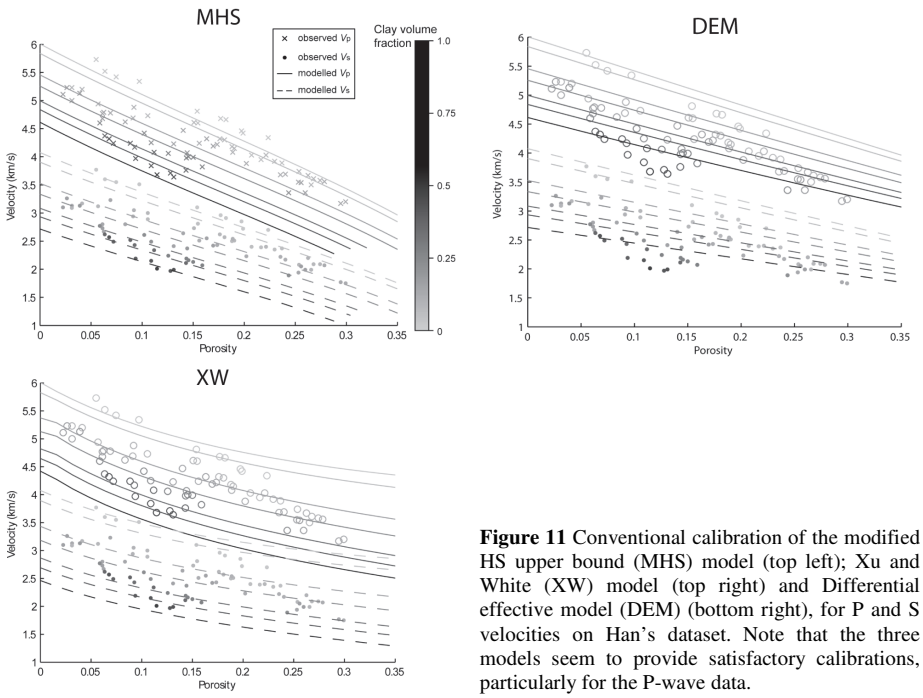

Figure 11 Conventional calibration of the modified HS upper bound (MHS) model (top left); Xu and White (XW) model (top right) and Differential effective model (DEM) (bottom right), for P and S velocities on Han's dataset. Note that the three models seem to provide satisfactory calibrations, particularly for the P-wave data.

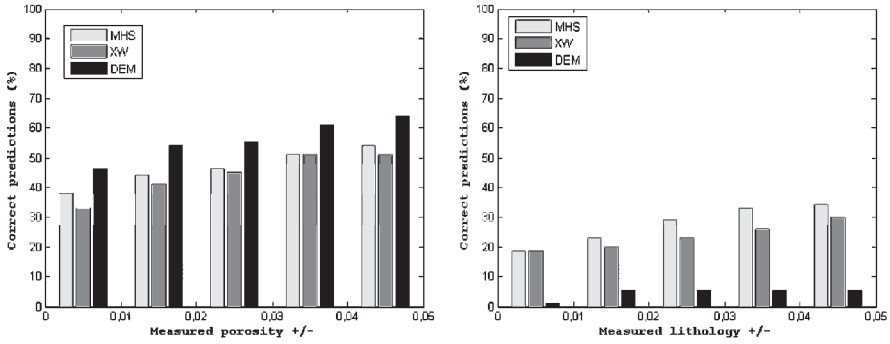

Figure 12 Results of the quantitative calibration of the modified Hashin-Shtrikman (MHS), Xu and White (XW) and differential effective modelling (DEM) models on Han's data set. Vertical axis is percentage of predictions matching the data, versus various tolerance ranges in porosity and lithology predictions (+/- 0.01, 0.02, 0.03, 0.04, 0.05) in the horizontal axis. Note the poor performance of the DEM model in terms of lithology.

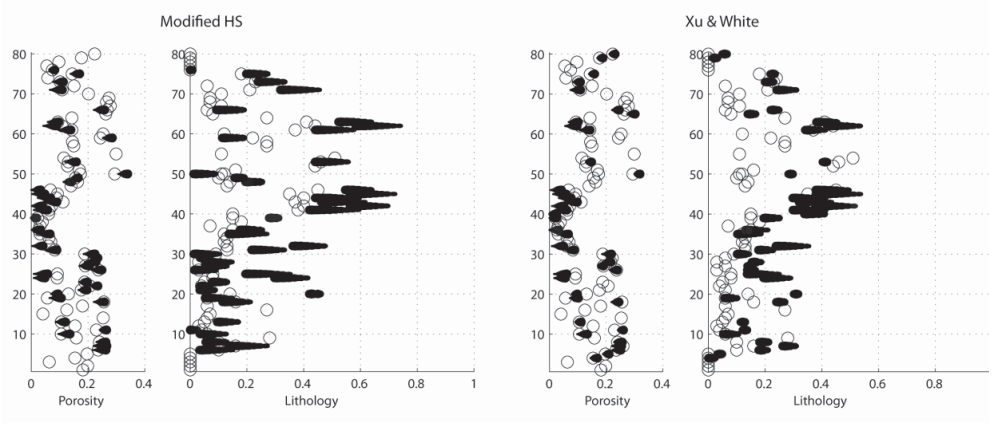

Figure 13. Quantitative calibration of the modified HS upper bound (MHS) on the left; Xu and White model (XW) on the right panel. Vertical axis is sample number, empty circles are lab measurements and filled circles model predictions. Note that both models provide a large number of accurate predictions.

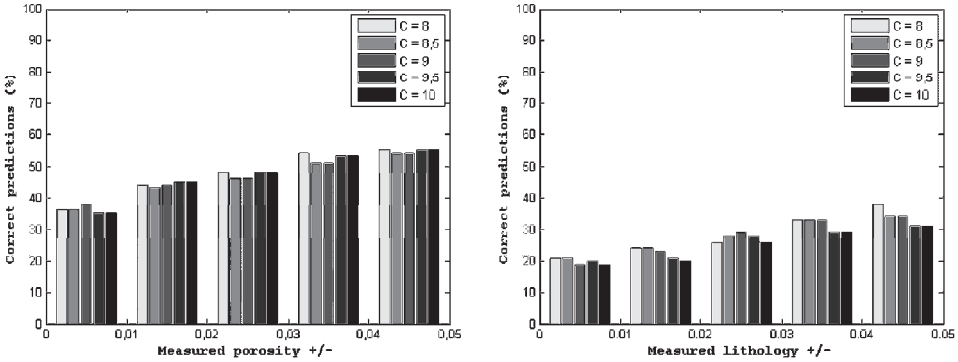

Figure 14 Improved calibration of the modified Hashin-Shtrikman model (MHS), on Han's data set for various coordination numbers (C). Vertical axis is percentage of predictions matching the data, versus various tolerance ranges in porosity and lithology (+/- 0.01, 0.02, 0.03, 0.04, 0.05) in the horizontal axis. Results are stable, and the calibration is not significantly dependent on coordination number.

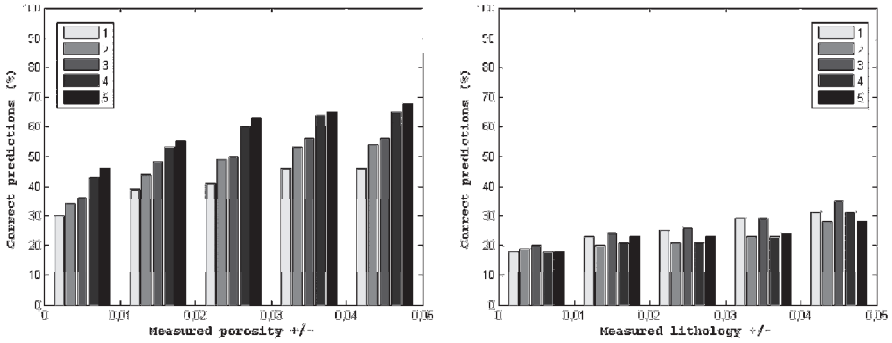

Figure 15 Improved calibration of the Xu and White model (XW), on Han's data set for various combinations of aspect ratios. Models 1 to 5 have aspect ratios (sand-pores, clay-pores) as follow: M1 = (0.1, 0.035); M2 = (0.1, 0.06); M3 = (0.12, 0.035); M4 = (0.12, 0.05); M5 = (0.12, 0.06). Vertical axis is percentage of predictions matching the data, versus various tolerance ranges in porosity and lithology (+/- 0.01, 0.02, 0.03, 0.04, 0.05) in the horizontal axis. Note that porosity predictions were optimized by using different aspect ratios whereas lithology maintains relatively stable.

DISCUSSION

The comparison between two models in the PLF space requires a conventional calibration of the models in a cross-plot domain, such as velocity-porosity space. This initial calibration step, however, can influence the first quantitative results in the PLF space. This ambiguity can be assessed by performing a (quantitative) sensitivity analysis (in the PLF space) for key parameters of each model (e.g., aspect ratios, pressure, and effective mineral properties), and selecting the combination of parameters that provides the higher number of solutions for the dataset under examination. After the optimal parameters have been found, further comparison with other models can be made.

The dataset used in the first case has been referenced in the literature to illustrate the effect of pore-filling clay on porosity and velocities of clay-sand mixtures. Its bimodal grain-size distribution and grain size ratio (1/20) suggest an ideal condition for a dispersed-clay microstructure. However, the predictions for the dispersed clay model were very sensitive to the uncertainty of the data. Overall, the structural-clay model produced a more robust set of predictions for both lithology and porosity. This can be explained from Figure 6. Where clay exceeds 10 % by volume, the dispersed model over-predicts P-velocity because structural clay becomes important in reducing the stiffness of the samples. This suggests that the effect of clay on the elasticity is predominantly inter-granular or structural, except for those with clay volumes below 10 % at which both dispersed and structural clay have similar impacts. This is likely related to the sample preparation procedures, and it is not a general condition of clay-rich sandstones. The quantitative analysis revealed this condition even though it was not evident from the conventional calibration process.

In the second case we used the quantitative calibration approach to select or discard the most suitable rock-physics models to reproduce a dataset. We compared the overall results of three models (MHS, XW and DEM) and were quickly able to discard the least accurate model (DEM). Through a sensitivity analysis of the remaining models, we explored the potential for optimizing the calibration in order to identify the model that provides the most stable and robust predictions. However, in cases with high uncertainty, where wide ranges of porosities and lithologies are expected, the model producing a wider range of results would be preferred. The dataset used in case 2 (Han's data) contains samples from various origins (quarries, well cores) with a wide range of porosities and clay contents, from clean tight sands to high porosity clay-rich sandstones. Therefore, dividing the dataset into more homogeneous subsets, for example in terms of origin, degree of consolidation, porosity or clay content, can improve the calibration and would allow inference of rock microstructure details from the model's success.

In both examples porosity predictions were more accurate than lithology predictions. Most observations of natural rocks indicate that elastic properties are more sensitive to

porosity than to lithology variations. Hence, higher correlations exist between velocity and porosity than between velocity and clay content. Variations of elastic moduli are more pronounced along porosity than lithology axes, which in turn produce less accurate predictions of lithology than porosity.

Our investigation in the PLF space included solutions with high water saturation (>90%) to simplify the analysis. In real cases, however, uncertainty in fluid saturation could lead to less accurate porosity and lithology predictions.

In order to compare the predictions of the different rock-physics models, in our examples we used only ultrasonic laboratory data, a procedure which provides maximum control of the lithology, porosity and saturation. But in a reservoir characterization context where predictions are evaluated in the scale of the field, a similar methodology could be used, calibrating the rock-physics models to log data up-scaled to seismic frequencies.

CONCLUSIONS

We applied an inverse modelling strategy that assesses the ability of a rock-physics model to predict porosity, lithology and saturation (PLF parameters) from seismic parameters. By analyzing the performance of the models in the PLF domain, we were able to select the model that provided the most robust estimations of reservoir properties. Additionally, in the first case we also diagnosed the dominant factor that affected elasticity of the samples.

We also illustrated how this quantitative approach can be used in a workflow to find a model for a large and heterogeneous dataset, considering a wide range of options, quickly discarding the less effective models and focusing on the most promising ones. Then, by testing several model parameters, we assessed the sensitivity of the selected models in terms of predictions of reservoir properties. This suggests that calibrating a rock-physics model only by best fitting in a cross plot domain, to relate inverted seismic data and reservoir parameters, can lead to inaccurate predictions of porosity and lithology. Analyzing the models in the PLF domain has the advantage of evaluating up to three seismic observables simultaneously and can point to inconsistencies in the model predictions between bulk and shear moduli. In conclusion, this is an integrated and robust approach to the inversion problem of finding the most appropriate rock physics model to explain measured data.

ACKNOWLEDGEMENTS

The authors acknowledge the Norwegian research council (NFR) for financial support through the Petromaks program and external sponsors (Statoil, Total, Rocksource). Moyano also would like to thank Statoil for granting a leave to pursue doctoral studies.

REFERENCES

Avseth, P., Mukerji, T., Mavko, G. & Dvorkin, J. 2010. Rock-physics diagnostics of depositional texture, diagenetic alterations, and reservoir heterogeneity in high-porosity siliciclastic sediments and rocks - A review of selected models and suggested work flows. *Geophysics* **75**, A31-A47.

Avseth, P., Mukerji, T. & Mavko, G. 2005. *Quantitative seismic interpretation: Applying rock physics tools to reduce interpretation risk*. Cambridge University Press.

Berge, P.A., Berryman, J.G., & Bonner, B.P. 1993. Influence of microstructure on rock elastic properties. *Geophysical Research Letters* **20**, 2619-2622.

Berryman, J.G. 1980. Long-wavelength propagation in composite elastic media I. Spherical inclusions. *Journal of the Acoustical Society of America* **68**, 1809-1819.

Berryman, J.G. 1992. Single-scattering approximations for coefficients in Biot equations of poroelasticity. *Journal of the Acoustical Society of America* **91**, 551-571.

Berryman, J.G. 1995. Mixture theories for rock properties. In: *Rock Physics and Phase Relations, AGU Reference Shelf 3, AGU, Washington, DC, 205-228* (ed. Ed. T.J.Ahrens), American Geophysical Union.

Digby, P.J. 1981. The effective elastic-moduli of porous granular rocks. *Journal of Applied Mechanics-Transactions of the Asme* **48**, 803-808.

Draege, A., Jakobsen, M. & Johansen, T.A. 2006. Rock physics modelling of shale diagenesis. *Petroleum Geoscience* **12**, 49-57.

Dvorkin, J. & Nur, A. 1996. Elasticity of high-porosity sandstones: Theory for two North Sea data sets. *Geophysics* **61**, 1363-1370.

Dvorkin, J. & Gutierrez, M.A. 2001. Textural sorting effect on elastic velocities, part II: Elasticity of a bimodal grain mixture. *SEG Technical Program Expanded Abstracts* **20**, 1764-1767.

Gassmann, F. 1951. Elastic waves through a packing of spheres. *Geophysics* **16**, 673-685.

Han, D., Nur, A. & Morgan, D. 1986. Effects of porosity and clay content on wave velocities in sandstones. *Geophysics* **51**, 2093-2107.

Hashin, Z. & Shtrikman, S. 1963. A variational approach to the theory of the elastic behaviour of multiphase materials. *Journal of the Mechanics and Physics of Solids* **11**, 127-140.

Hill, R. 1952. The elastic behaviour of a crystalline aggregate. *Proceedings of the Physical Society of London Section A* **65**, 349-355.

Hornby, B.E., Schwartz, L.M. & Hudson, J.A. 1994. Anisotropic effective-medium modeling of the elastic properties of shales. *Geophysics* **59**, 1570-1583.

Hudson, J.A. & Knopoff, L. 1989. Predicting the overall properties of composite-materials with small-scale inclusions or cracks. *Pure and Applied Geophysics* **131**, 551-576.

Jakobsen, M., Hudson, J.A. & Johansen, T.A. 2003. T-matrix approach to shale acoustics. *Geophysical Journal International* **154**, 533-558.

Johansen, T.A., Ruud, B.O. & Jakobsen, M. 2004a. Effect of grain scale alignment on seismic anisotropy and reflectivity of shales. *Geophysical Prospecting* **52**, 133-149.

Johansen, T.A., Spikes, K. & Dvorkin, J. 2004b. Strategy for estimation of lithology and reservoir properties from seismic velocities and density. *SEG Technical Program Expanded Abstracts* **23**, 1726-1729.

Kuster, G.T. & Toksoz, M.N. 1974. Velocity and attenuation of seismic-waves in 2-phase media I. Theoretical Formulations. *Geophysics* **39**, 587-606.

Marion, D., Nur, A., Yin, H. & Han, D. 1992. Compressional velocity and porosity in sand-clay mixtures. *Geophysics* **57**, 554-563.

Mindlin, R.D. 1949. Compliance of elastic bodies in contact. *Journal of Applied Mechanics-Transactions of the Asme* **16**, 259-268.

O'Connell, R.J. & Budiansky, B. 1974. Seismic velocities in dry and saturated cracked solids. *Journal of Geophysical Research* **79**, 5412-5426.

Sheng, P. 1990. Effective-medium theory of sedimentary-rocks. *Physical Review B* **41**, 4507-4512.

Walton, K. 1987. The effective elastic-moduli of a random packing of spheres. *Journal of the Mechanics and Physics of Solids* **35**, 213-226.

Xu, S.Y. & White, R.E. 1995. A new velocity model for clay-sand mixtures. *Geophysical Prospecting* **43**, 91-118.

Yin, H. 1992. *Acoustic velocitiy and attenuation of rocks, isotropy, intrinsic anisotropy, and stress induced anisotropy*. Ph.D. dissertation, Stanford University.